Heliyon 9 (2023) e12890

Contents lists available at ScienceDirect

Heliyon

journal homepage: www.cell.com/heliyon

Research article

Bionics design of affinity peptide inhibitors for SARS-CoV-2 RBD to block SARS-CoV-2 RBD-ACE2 interactions

Xiaofeng Liu [a,b], Luying Jiang [a,b], Li Li [c], Fuping Lu [a,b], Fufeng Liu [a,b,*]

[a] Key Laboratory of Industrial Fermentation Microbiology of Ministry of Education; Tianjin Key Laboratory of Industrial Microbiology, PR China
[b] College of Biotechnology, Tianjin University of Science & Technology, Tianjin 300457, PR China
[c] College of Marine and Environmental Science, Tianjin University of Science & Technology, Tianjin 300457, China

ARTICLE INFO

Keywords:
SARS-COV-2
Molecular dynamics simulation
Molecular docking
Bionic design
Short peptide inhibitors

ABSTRACT

Coronavirus Disease 2019 (COVID-19), has already posed serious threats and impacts on the health of the population and the country's economy. Therefore, it is of great theoretical significance and practical application value to better understand the process of COVID-19 infection and develop effective therapeutic drugs. It is known that the receptor-binding structural domain (SARS-CoV-2 RBD) on the spike protein of the novel coronavirus directly mediates its interaction with the host receptor angiotensin-converting enzyme 2 (ACE2), and thus blocking SARS-CoV-2 RBD–ACE2 interaction is capable of inhibiting SARS-CoV-2 infection. Firstly, the interaction mechanism between SARS-CoV-2RBD-ACE2 was explored using molecular dynamics simulation (MD) coupled with molecular mechanics Poisson-Boltzmann surface area (MM-PBSA) free energy calculation method. The results of energy analysis showed that the key residues R403, R408, K417, and Y505 of SARS-CoV-2 RBD and the key residues D30, E37, D38, and Y41 of ACE2 were identified. Therefore, according to the hotspot residues of ACE2 and their distribution, a short peptide library of high-affinity SARS-CoV-2 RBD was constructed. And by using molecular docking virtual screening, six short peptides including DDFEDY, DEFEDY, DEYEDY, DFVEDY, DFHEDY, and DSFEDY with high affinity for SARS-CoV-2 RBD were identified. The results of MD simulation further confirmed that DDFEDY, DEYEDY, and DFVEDY are expected to be effective inhibitors. Finally, the allergenicity, toxicity and solubility properties of the three peptide inhibitors were validated.

1. Introduction

Coronavirus Disease 2019 (COVID-19), has spread across the globe, imposing a heavy burden on society and the economy. Previous studies have shown that COVID-19 has a high degree of homology with SARS in 2003, so it was also named severe acute respiratory syndrome coronavirus 2 (SARS-COV-2) [1]. The family *Coronaviridae* is in the order *Nidovirales*. Members of this family are positive-sense single-stranded RNA viruses that are genetically categorized into the genera α-coronavirus, β-coronavirus, γ-coronavirus, and δ-coronavirus [2,3]. SARS-CoV-2 is derived from β-coronavirus, and its gene mainly encodes four structural proteins: the nucleocapsid protein, the membrane protein, the envelope protein, and the spike protein [4]. Among them, the spike protein plays an

* Corresponding author. Key Laboratory of Industrial Fermentation Microbiology of Ministry of Education; Tianjin Key Laboratory of Industrial Microbiology, PR China.
E-mail address: fufengliu@tust.edu.cn (F. Liu).

https://doi.org/10.1016/j.heliyon.2023.e12890
Received 18 August 2022; Received in revised form 30 December 2022; Accepted 6 January 2023
Available online 13 January 2023

critical role in infection and entry into host cells [5]. The spike protein is club-shaped and exists as a trimer, with each monomer consisting of two domains (S1 and S2). While the S2 domain is embedded in the viral membrane, the S1 domain is exposed to the surface [6]. Previous studies revealed that the spike protein can exist in three conformational states: open (or up), semiopen and closed (or down) [7,8]. These conformations refer to the structure of the receptor-binding domain (RBD, residues 319–541) found on the S1 domain [7,9]. Recent studies have shown that SARS-CoV-2 RBD first interacts with angiotensin-converting enzyme 2 (ACE2), induces the virus to fuse with the host cell membrane, allowing the coronavirus to infect the host cell [10,11]. Notably, SARS-CoV-2 RBD directly mediated the interaction with ACE2 to complete the infection process [12,13]. In addition, previous studies have shown that the host's ability to be infected with SARS-CoV mainly depends on the affinity between RBD and host receptor ACE2 [141516171819]. Therefore, the development of inhibitors that inhibit SARS-CoV-2 RBD-ACE2 protein-protein interactions could effectively block the interactions, which is critical in the response to SARS-COV-2.

At present, molecular dynamics (MD) simulation has emerged as the most common yet obvious method to investigate biomolecular interactions and conformational dynamics [20]. MD simulation-based binding free energy calculations has proven valuable. Mandal et al. [21] compared the RBD-ACE2 complex of the Variants of Concern with the Wild Type system by using all-atom MD simulations. It was observed that electrostatic interactions play a major role in the binding of the complexes. Similarly, by using all-atom MD simulations, Rath et al. [22] compared the interaction of Wild-type RBD-ACE2 complex with that of the latest Omicron variant of the virus. The residue wise interaction energies of the mutated residues and surface electrostatics imply that this energy change is favorable for the binding of ACE2 and the stability of the Omicron when compared to Wild-type. Inevitably, performing biochemical experiments on SARS-CoV-2 is time-consuming and requires sophisticated security operation. In the context of SARS-CoV-2, computational approaches have been widely used to predict binding affinities and evaluate the interactions that occur between protein-ligand and protein-protein complexes at the molecular level [23,24]. For instance, docking, ADMET properties calculation, MD and molecular mechanics Poisson-Boltzmann surface area (MM-PBSA) approaches were coupled to check the therapeutic potentials of N. sativa chief constituents against COVID-19 [25]. Kumar et al. [26] have screened FDA approved 2466 drugs against the predicted binding site at the RBD-ACE2 interface, leading to 6 drugs exhibited stable binding with RBD at the RBD-ACE2 interface after the verification of MD simulations. The computational studies are quick and easily performed to provide COVID-19 information.

Except for small compounds, peptide inhibitors have been considered a major hotspot for drug development due to their high affinity to proteins, low toxicity, high inhibitory capacity and ease of synthesis [27]. Designing novel peptide inhibitors that can inhibit viral binding to ACE2 and prevent the virus from invading cells, is a possible treatment strategy. Jaiswal et al. [28] have identified a double helical inhibitor amantadine binding protein (ΔABP)-D25Y that binds at the receptor binding motif site of SARS-CoV-2 RBD with higher affinity than ACE2. Based on the known ACE2 binding sites on RBD, Cao et al. [29] developed two novel peptides named LCB1 and LCB3 with high binding affinity to the SARS-CoV-2 RBD and high neutralizing ability. However, the above peptides are still considered as large-size inhibitors, with ΔABP-D25Y, LCB1, and LCB3 having 60, 56, and 64 residues, respectively. In this regard, designing some smaller peptides would be more desirable since it will lower manufacturing costs with higher output and easier penetration into tissues and cells with high specificity. The allergenicity, toxicity, and solubility of peptides were assessed via bioinformatics tools to verify the validity and potency of the construct. Campos et al. [30] identified the 7 mutations with strong binding affinity, high antigenicity, allergenicity, immunogenicity, and nontoxicity present in spike protein of all SARS-CoV-2 variants that we could readily use in the construction of prototype peptide vaccine. A novel multi-epitopes peptide vaccine construct against the Jaagsiekte retrovirus, Mahmoud et al. [31] predicted that these peptide vaccines include antigenicity, sensitization, toxicity, and stability. This type of analysis saves time, resources, and money for the pharmaceutical and vaccine industries [32].

In this work, molecular docking and MD simulation were used to design short peptide inhibitors that disrupt the binding of SARS-CoV-2 RBD to ACE2. First, the interaction and key residues were investigated. Then, short peptide inhibitors with a high affinity for SARS-CoV-2 RBD were designed based on the distribution of key residues using molecular docking. Secondly, MD simulations were performed to verify the affinity between the short peptide inhibitors and SARS-COV-2 RBD. Finally, the predicted results of bioinformatics tools showed that these peptides had no allergenicity, no toxicity and good water solubility. The novel peptides developed here as well as the overall strategy have a strong potential to lead to generally applicable anti-COVID-19 therapeutics.

2. Materials and methods

2.1. Molecular dynamics simulation

The complex conformation of SARS-CoV-2 RBD-ACE2 was obtained from the Protein Data Bank database with PDB ID 6LZG [33]. Topology files of short peptides were generated using the ATB [34] website, and Gromos 54A7 force field [35] was selected.

GROMACS 5.1.4 was used to analyze the movement of the complex structure in the all-atomic field of CHARMM27 [36]. First, a cubic box with a volume of 2343.04 nm^3 was constructed, so that the proteins in the neighbor periodic box are at least 1.5 nm apart from each other. Then periodic boundary conditions were used. The remaining space in the box was filled with TIP4P [37], and 24 Na^+ ions were added to balance charges. All molecules in the systems were optimized by steepest descent minimization performed for 5000 steps with a maximum force constant value of 1000 kJ/mol/nm. After the geometrical optimization, the systems were equilibrated in isothermal isometric (NPT) ensemble for 100 ps at a timestep of 2 fs. The temperature of 310 K and the pressure of 1 atm were maintained by the Berendsen thermostat and the Parrinello-Rahman barostat [38], respectively. Particle Mesh Ewald (PME) method [39] was used to treat the long-range electrostatic interactions with a real space cutoff of 1.0 nm. The *van der Waals* interactions [40] were also cut off at 1.0 nm, with the appropriate cutoff corrections added to pressure and energy. All hydrogen bonds were constrained by the LINCS method [41]. After the equilibration, 100 ns MD production run at a timestep of 2 fs was performed for statistics.

2.2. Data analysis

All trajectories were analyzed using the GROMACS package's built-in programs and related plug-ins. The *gmx rms* and *gmx mindist* command were applied to calculate the root-mean-square deviation (RMSD) of the target protein and the distance between ligand and the target protein, respectively. The *g_mmpbsa* command [42] was applied to analyze the energy [43]. In addition, all images were rendered by applying the Visual Molecular Dynamics (VMD) software (http://www.ks.uiuc.edu/Research/vmd/) [44].

2.3. Bionic design of short peptide inhibitors

The distance between the C-terminal and N-terminal of key residues of ACE2 was calculated using VMD software. Then, to design the molecular model of short peptide inhibitors, 20 common amino acids were docked with the gaps formed by the key residues of SARS-CoV-2 RBD by using AutoDock [45]. The filling process refers to previous researches [46,47]. And then, to screen out the short peptide inhibitors with high affinity to SARS-CoV-2 RBD, the candidate short peptide inhibitors were docked with the whole SARS-CoV-2 RBD using Vina [48].

2.4. Docking

AutoDock [45] and Vina [48] were used to design short peptides with a high affinity to SARS-CoV-2 RBD. The AutoDock software is composed of the AutoGrid program responsible for calculating the relevant energy in the grid and the AutoDock program responsible for conformation search and evaluation of their affinity [49]. The receptor was treated as rigid entity whereas ligands were kept flexible to obtain the best fitting conformation with respect to the receptor complex. First, AutoDock was used to dock 20 common amino acids to the target regions of SARS-COV-2 RBD. Here, the grid spacing was set as 0.375 Å, and the center of the grid points was x $= -31.606$, y $= 33.577$, z $= 11.244$. The grid size boundaries along X, Y, and Z axes were set as 40 Å $\times$ 80 Å $\times$ 40 Å, and the number of conformations obtained by docking is 300. Then, Vina software was used to perform docking screening for alternative short peptide inhibitors. Among them, the grid spacing was set as 1 Å, and the center of the grid points is x $= -32.358$, y $= 29.77$, z $= 21.005$. The grid size boundaries along X, Y, and Z axes were set as 40 Å $\times$ 45 Å $\times$ 55 Å, and the number of conformations obtained by docking was 10.

2.5. Binding free energy calculations using MM-PBSA analysis

MM-PBSA analysis was used to calculate the free energy of binding (ΔG_{bind}) of the SARS-COV-2 RBD-ACE2 complex using *g_mmpbsa*. In MM-PBSA, the enthalpy change of the system is calculated by molecular mechanics (MM) method [50], the contribution of polar part to free energy in solvent effect is calculated by solving Poisson-Boltzmann (PB) equation [51], the contribution of the non-polar part of the solution effect to the free energy is calculated by the molecular accessible surface area (SASA) [52]. The basic principle is as follows:

$$\Delta G_{bind} = \Delta E_{MM} + \Delta\Delta G_{sol} - T\Delta S$$

The binding free energy of SARS-CoV-2 RBD and ACE2 was calculated on the finally 10 ns of MD simulation trajectories taking 200 configuration snapshots. The per-residue energy contribution of the complexes was also estimated. The binding free energy of the system was estimated through the following equation,

$$\Delta G_{bind} = \Delta E_{elec} + \Delta E_{vdw} + \Delta G_{PB} + \Delta G_{SASA} - T\Delta S$$

The formula, ΔG_{bind} is the binding free energy, ΔE_{MM} is the intramolecular energy in vacuum, including electrostatic interaction (ΔE_{elec}), *van der Waals* force (ΔE_{vdw}), and Δ ΔG_{sol} is solvation free energy, including polar solvation energy (ΔG_{PB}) (calculated by PB equation) and non-polar solvation energy (ΔG_{SASA}) (obtained by calculating molecular accessible surface area). The entropic energy ($T\Delta S$) is usually ignored because of its estimation is a slow process and yields a small value [53]. In this study, the binding free energy of the complex does not include the energy contributed by entropy.

2.6. Allergenicity, toxicity and solubility prediction tool of peptides

AllerTOP V.2 [54] (http://www.ddg-pharmfac.net/AllerTOP/), a novel model for allergen prediction using machine learning approaches, has been widely used to predict the allergenicity. The allergenic potential was evaluated using the AllerTOP V.2 web server by applying auto-cross covariance transformation to build a dataset of known allergens and developing alignment-independent models for allergen recognition based on the physicochemical properties of peptides. The tool uses five machine learning methods for protein classification, including partial least squares discriminant analysis, logistic regression, decision tree, naïve Bayes, and k-nearest neighbors. In addition, AllerTOP V.2 attempts to identify the most likely route of exposure AllerTOP V.2 outperforms other allergen prediction models, with a sensitivity of 94% [47]. AllerTOP V.2 was used to search for identical short (6–8) amino acid segments of the query protein that exactly match any segment of a known allergenic protein. ToxinPred [55] (http://crdd.osdd.net/raghava//toxinpred/) was used to distinguish the toxicity of peptides. It uses the following datasets to train and test SVM models: (1) a main dataset (1805 toxin sequences from experimentally validated peptides/proteins (positive examples) and 3593 non-toxin sequences

from SwissProt (negative examples)), (2) a main independent dataset (303 toxin sequences and 300 SwissProt non-toxin sequences), (3) an alternative dataset (1805 toxin sequences (positive examples) and 12,541 non-toxin sequences from TrEMBL (negative examples)), (4) and an alternative independent dataset (303 toxin sequences from SwissProt and 1000 non-toxin sequences from TrEMBL). Solubility is the measure of homogeneity of the system from the mixture of solute and solvent. It is considered as one of the vital parameters in drug concentration determination for a desired pharmacological response [56]. Poor solubility of drugs is a major issue in drug discovery and development. Solubility acts as a driving force to attain high drug concentration in blood for therapeutic effectiveness [57]. The solubility property of affinity peptides can be obtained from the peptide property calculator PepCalc.com (http://pepcalc.com/), which is freely available online and has been widely used.

3. Results and discussion

3.1. Structural stability of SARS-CoV-2 RBD and ACE2 complex

RMSD value is often used to indicate the structural stability of the protein. The smaller the fluctuation of the RMSD value, the more stable the structure of the protein. Therefore, to judge whether the balance between ACE2 and SARS-CoV-2 RBD had been reached, the RMSD value of the complex was calculated (Fig. 1A).

In Fig. 1A, the RMSD values rise rapidly at the early stage of the simulations, and fluctuated wildly within the following time. It indicates that initial conformation of the complex is not optimal, and they constantly adjust and optimize conformation to fit each other. In the last 50 ns, the fluctuation of RMSD value is relatively stable, which implies the complex conformation reaches a steady state. To assess the stability of the bound complexes and their conformations due to binding, superimposition of the initial structure and the final structure (averaged over the MD trajectory) of the SARS-CoV-2 and ACE2 complexes was performed and shown in Fig. 1B. Therefore, we chose the last 10 ns of simulation to calculate the binding energy. We only estimate the energy between residues at the binding interface of SARS-CoV-2 RBD and ACE2 in Fig. 2 due to computational requirements. As shown from the figure, ACE2 is closely integrated with SARS-COV-2 RBD.

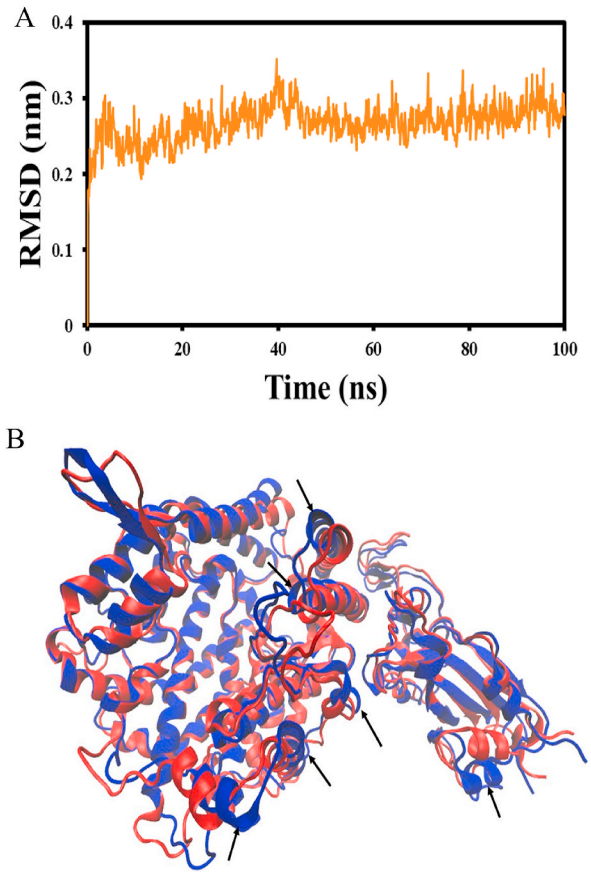

Fig. 1. The structural stability of the complex. The time evolution of RMSD values of SARS-CoV-2 RBD-ACE2 conformation (A). Superimposition of the initial (blue) and final (red) structures of SARS-CoV-2-ACE2 complex in MD simulations (B). Black arrows point to conformational deviations.

3.2. Free energy analysis based on MD simulation

Previous studies have shown a significant error in the energy analysis based on a single conformation, but MD simulation can significantly reduce that [58,59]. Therefore, we also used MD simulation combined with the MM-PBSA method to calculate the total energy, and decomposed the binding free energy into four terms: *van der Waals* energy, electrostatic energy, polar solvation energy, and nonpolar solvation energy.

Table 1 shows the energies between the binding interface of SARS-CoV-2 RBD and ACE2 in the last 10 ns. The total energy reach -364.70 ± 64.74 kJ/mol, which indicates that there is a stronger binding tendency between them. It is easy to see that the electrostatic interactions (-603.08 ± 72.94 kJ/mol) contribute the most of binding free energies in complexes of ACE2 with SARS-CoV-2 RBD, which is about 2 times higher than the *van der Waals* energy (-305.02 ± 19.75 kJ/mol). However, the electrostatic energy is mainly offset by the polar solvated free energy (583.51 ± 104.67 kJ/mol). Thus, the non-polar energy composed of *van der Waals* energy (-305.02 ± 19.75 kJ/mol) and SASA energy (-40.10 ± 2.37 kJ/mol) plays an important role in their binding. Considering their physical and chemical properties, it can be found that ACE2 possesses 27 negative charges, and SARS-CoV-2 RBD possesses 2 positive charges. Therefore, this may be one of the reasons why the high electrostatic energy value. The strong electrostatic energy between them results in strong protein-protein interactions.

Therefore, it can be concluded that both the non-polar and polar energy are the main forces promoting the interactions between SARS-CoV-2 RBD and ACE2, among which the electrostatic energy cannot be ignored. And our results are consistent with that of Cao et al. [60].

3.3. Free energy decomposition

Not only is the MM-PBSA method often used to evaluate the interaction energy between protein and protein, but its energy decomposition can also be used to identify key residues of proteins [46,58,59]. To further analyze the energy contribution of each residue at the protein-binding interface, we decompose the binding energy into the energy contributed by each residue.

Herein, residues whose absolute value of energy contribution is less than 5 kJ/mol are ignored. Fig. 3 reports the specific energy values contributed by residues of SARS-CoV-2 RBD-ACE2 and the distribution of these residues. As can be seen from Fig. 3, there are a large number of polar residues at their binding interface, and these polar residues contribute highly high energy. According to protein–protein interaction results, it is clear that the critical residues are predominantly on the α-helix of the ACE2. The 18 critical residues E22, E23, T27, F28, D30, E35, E37, D38, Y41, E56, E57, D67, E75, M82, E329, D335, D350, and D355 (Fig. 3B) in ACE2 have an important role in interactions of SARS-CoV-2 RBD, which is almost similar to the binding residues profile of ACE2 interface reported previously [61,62]. In addition, some residues with the ring also contribute to considerable non-polar energy. Whereas the hotspot residues in the SARS-CoV-2 RBD including R403, R408, K417, K424, K444, R454, L455, F456, R457, K458, K462, R466, F486, and Y505 are identified, which were in line with the findings of Yan et al. [6] Form Fig. 3A, the positively charged residues of SARS-CoV-2 RBD are favorable for the combination of SARS-CoV-2 RBD and ACE2, while negatively charged residues have the opposite effect. In contrast, negatively charged residues of ACE2 contribute favorable energy, while positively charged residues are unfavorable for their binding (Fig. 3B). This is also the reason why the electrostatic energy is far greater than the sum of *van der Waals* energy and SASA energy (Table 1), and the electrostatic energy is mainly contributed by these residues. It consistent with an overall more compatible electrostatic interactions between RBD and ACE2 in the complex of SARS-CoV-2 than that in SARS-CoV [6].

In addition, the energy contributed by the residues of SARS-CoV-2 RBD is much greater than that of ACE2. Thus, it can be inferred

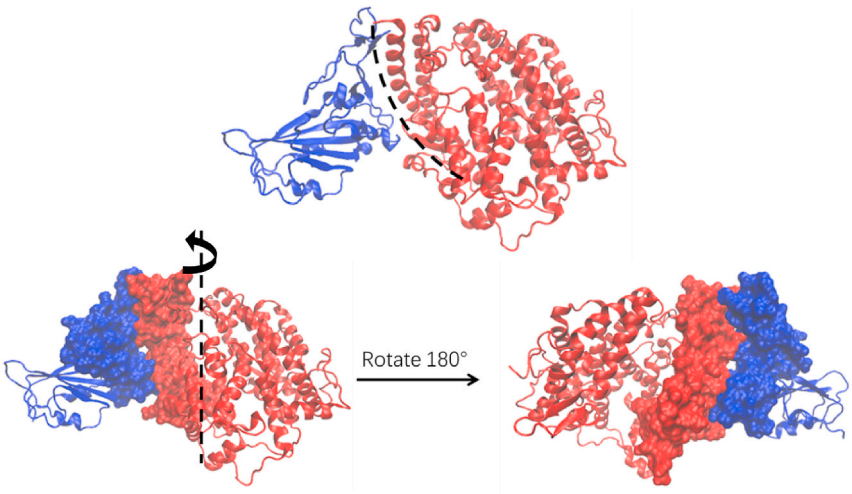

Fig. 2. Three-dimensional structure of the complex conformation of SARS-CoV-2 RBD-ACE2. SARS-CoV-2 RBD and ACE2 were rendered in blue and red NewCartoon, respectively. Among them, these residues of the interface were rendered in blue and red Surf, respectively.

Table 1
The binding energy between SARS-CoV-2 RBD and ACE2, calculated from finally 10 ns molecular dynamics simulations.

Energy components	complex (kJ/mol)
Van der Waals	−305.02 ± 19.75
SASA	−40.10 ± 2.37
Electrostatic	−603.08 ± 72.94
Polar solvation	583.51 ± 104.67
Binding	−364.70 ± 64.74

* Polar = Polar solvation.
* Nonpolar = *Van der Waals* + SASA + Electrostatic.
*Binding = Polar + Nonpolar.

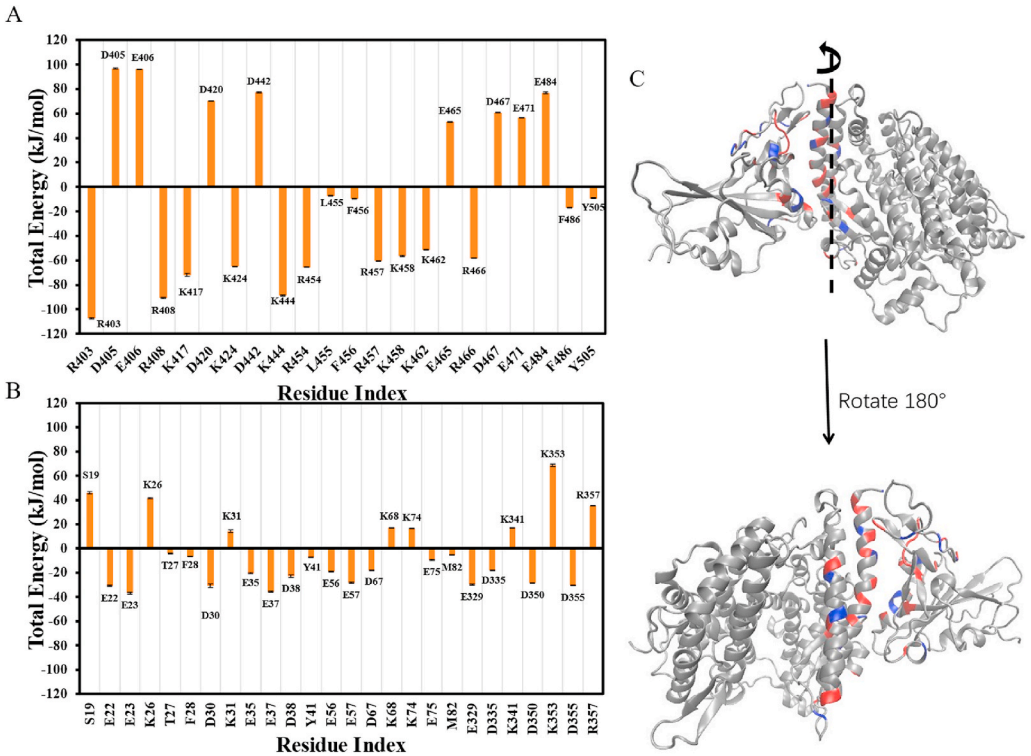

Fig. 3. Binding energy decomposition. Herein, residues whose absolute value of energy is less than 5 kJ/mol are ignored. Specific energy values contributed by residues of SARS-CoV-2 RBD (A) and ACE2 (B). Distribution of residues of SARS-CoV-2 RBD and ACE2 (C), where the residues contributing favorable energy are shown in red, and the unfavorable energy are shown in blue.

that the residues of SARS-CoV-2 RBD play a key role in their combination (Fig. 3A and B). On the one hand, most polar residues contribute favorable energy to their combination. On the other hand, hydrophobic residues (such as residues T27, F28, Y41, and M82 of ACE2 and residues L455, F456, F486, and Y505 of SARS-CoV-2 RBD) also provide considerable non-polar energy. A large number of polar residues at the interaction interface suggested that electrostatic energy is the main factor, which is consistent with the findings of Wang et al. [63] The high-affinity interactions between them are caused by multiple residues of the binding interface. Previous study found that SARS-CoV-2 RBD was mainly recognized by ACE2 through polar residues [7], which is consistent with our results.

Due to the negatively charged residues of ACE2 contribute favorable energy, the negative charged residues of SARS-CoV-2 RBD show highly repulsive energy values. The negatively charged residues of SARS-CoV-2 RBD are surrounded by the same charged residues in ACE2, and thus electrostatic repulsion may easily occur between them to prevent the binding of the SARS-CoV-2 RBD to ACE2. Moreover, mutations in these negatively charged residues of RBD are often accompanied by enhanced transmissibility and virulence of SARS-CoV-2 [64]. For example, the residue variation of E484 plays an important role in the stronger ACE2 binding affinity. E484K in both Alpha and Beta variants of Spike-RBD would increase the binding energy to −226.64 ± 2.8 and −258.40 ± 4.71 kJ/mol, respectively. However, E484 in the WT and Gamma variants show highly repulsive energy values (212.50 ± 1.1 and 199.02 ± 0.84 kJ/mol respectively) indicating there are unfavorable interactions between them [21].

3.4. Design of short peptides with high affinity for SARS-CoV-2 RBD

Based on the results in Fig. 3, the best binding site of the short peptide inhibitors was determined and shown in Fig. 4A. The grooves that are conducive to the binding of short peptide inhibitors can be observed at the binding interface (Fig. 4A). The key residues R403, R408, K417, and Y505 of SARS-CoV-2 RBD and the key residues D30, E37, D38, and Y41 of ACE2 were also recognized, according to the energy decomposition in Fig. 3, and the distribution of these key residues was shown in Fig. 4B. As shown from Fig. 4B, the key residues of SARS-CoV-2 RBD are almost in one-to-one correspondence with that of ACE2. These key residues are located at the interaction interface, and are critical for their combination.

Short peptides with a strong affinity for SARS-CoV-2 RBD were designed according to the distribution of key residues. Herein, we refer to previous researches, including amino acid localization and fragment linking methods [46,47] to construct short peptides. Fig. 4C shows the distribution of four key residues of ACE2 and the distance between the C-terminal and N-terminal of some residues. According to free energy decomposition and pair interaction analysis [46], four key residues D30, E37, D38, and Y41 of ACE2 were identified. Therefore, the molecular model (DX1X2EDY) of short peptide inhibitors was designed, where "X" can represent any one of 20 common amino acids.

Subsequently, 20 common amino acids were docked with the key regions formed by residues V401–N422, Y453–F456, and F490–Y505 of SARS-CoV-2 RBD, respectively. Due to X1X2 are inserted into the molecular motif (DX1X2EDY), which is built based on the binding fragment D30-E37 of ACE2, the RBD of SARS-CoV-2 were divided into two binding regions, region I and region II (Fig. 5A). According to the energy score and position of each amino acid after docking, the amino acid bound in region I is defined as "X1" and the amino acid bound in region II is defined as "X2". The binding energy is shown in Fig. 5B. “X1” amino acid was replaced with D, C, Q, and E; X2 amino acid was replaced with A, R, E, H, I, L, K, M, F, S, T, W, Y, and V, a total of 74 “DX1X2EDY” short peptide library was obtained. Finally, 74 short peptides were docked to identify the potential inhibitors for the RBD of SARS-CoV-2. Although all of the molecules bind actively with the SARS-CoV-2 RBD, but 6 affinity short peptides (DDFEDY, DEFEDY, DEYEDY, DFVEDY, DFHEDY, and

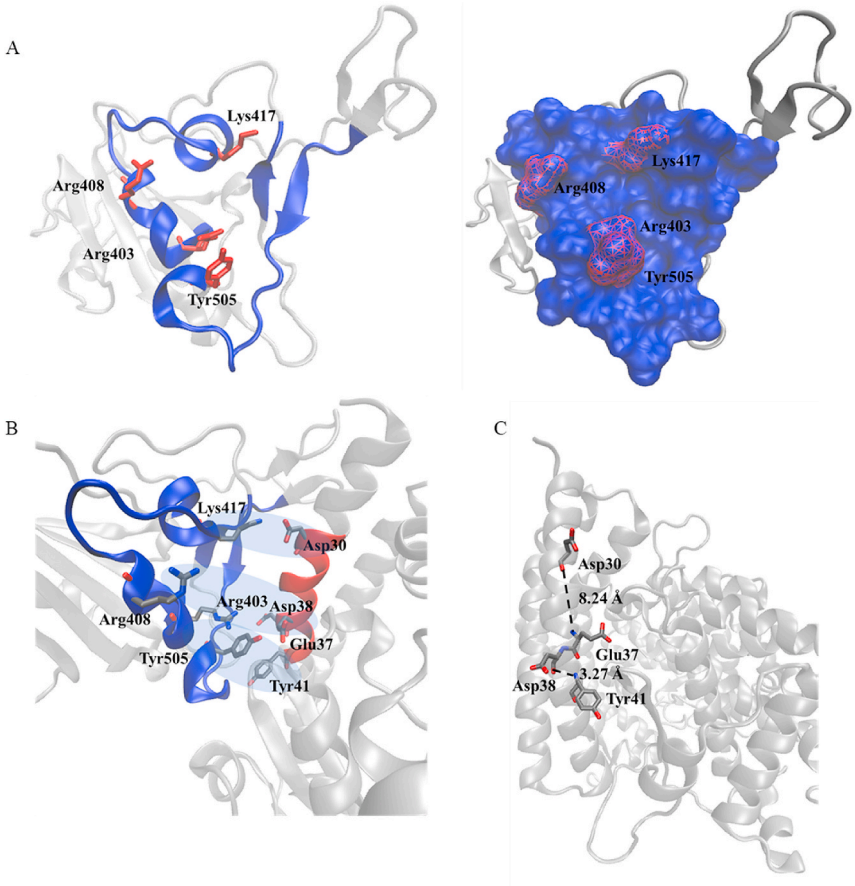

Fig. 4. Design of short peptide inhibitors. The grooves formed by residues V401–N422, Y453–F456, and F490–Y505 of SARS-CoV-2 RBD (A). The groove was rendered in blue NewCartoon and Surf, respectively, and the key residues were represented in red Licorice and Surf, respectively. Distribution of key residues of SARS-CoV-2 RBD and ACE2 (B). SARS-CoV-2 RBD, ACE2, and the key residues were displayed in blue NewCartoon, red NewCartoon, and Licorice, respectively. Distribution of four key residues of ACE2 and the distance between C-terminal and N-terminal of the residues (C).

A

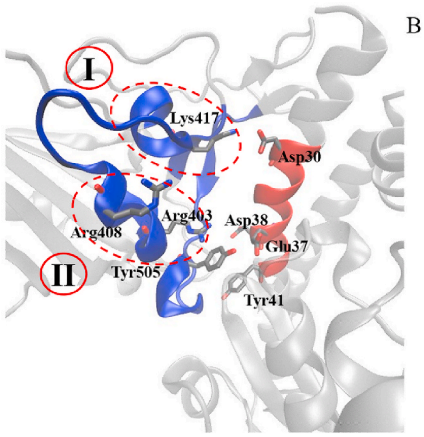

B

	Region I docking energy (kJ/mol)	Region II docking energy (kJ/mol)
Ala		-3.04
Arg		-3.62
Asn		
Asp	-3.57	
Cys	-3.04	
Gln	-3.97	-3.45
Glu	-3.83	
Gly		
His		-5.08
Ile		-3.71
Leu		-4.10
Lys		-3.40
Met		-3.72
Phe	-4.58	-5.37
Ser	-2.27	-3.20
Thr		-2.61
Trp		-4.84
Tyr		-4.35
Val		-3.49

Fig. 5. The potential amino acids in X1 and X2. Two binding regions, region I and region II, were selected from residues V401–N422, Y453–F456 and F490–Y505 of SARS-CoV-2 RBD. Region I and region II were set inside the red dashed line circle, respectively (A). The binding energy and positions of 20 amino acids, respectively (B).

DSFEDY) have the highest binding affinity.

3.5. Verification of the affinity between short peptides and SARS-CoV-2 RBD

Because docking software only considers the flexibility of the ligands, and usually ignores the effect of solvation effect, the calculations of affinity between ligands and proteins are often inaccurate [656667]. To further verify whether the short peptides have a high affinity with SARS-COV-2 RBD, MD simulation was carried out. Early studies reported that ligand-protein complex could reaches balance in 100 ns. [686970]. Therefore, we also use 100 ns MD simulation to verify the affinity.

Fig. 6 shows the average value of the minimum distance between short peptides and SARS-CoV-2 RBD. And the value is between 0.17 and 0.19 nm in six simulation systems, which suggests these short peptides and SARS-CoV-2 RBD have always maintained a relatively balanced state, and these short peptides are not far away from SARS-CoV-2 RBD. Moreover, to further observe whether the short peptides have moved away from the binding interface of SARS-CoV-2 RBD, the typical conformations of the short peptides-SARS-CoV-2 RBD at 100 ns were analyzed (Fig. 7). It can be found that DDFEDY, DEYEDY, and DFVEDY are located at the interface, while DEFEDY, DSFEDY, and DFHEDY tend to stay away from that (the blue region in Fig. 7), which indicate that these short peptides, including DDFEDY, DEYEDY, and DFVEDY are more likely to bind and remain on the interface and have high affinity with SARS-COV-2 RBD. Therefore, DDFEDY, DEYEDY, and DFVEDY are expected to be effective inhibitors to prevent the protein-protein interactions between SARS-CoV-2 RBD and ACE2.

To explore the affinity between these short peptides and SARS-CoV-2 RBD, we used the MM-PBSA to calculate the total binding energies of the protein complexes in Table 2. The last 10 ns of simulated trajectories of all the systems was used for MM-PBSA based binding energy calculations. Table 2 shows the binding energies of the four systems under study. DEYEDY and DDFEDY complexes showed average binding free energy -456.66 ± 41.17 and -388.92 ± 48.75 kcal/mol, while the average binding free energy of DFVEDY was -315.87 ± 31.45 kcal/mol. It is observed that for both SARS-CoV-2 RBD and short peptide, electrostatic energy plays a crucial role in the interaction process. The *van der Waals* energy, electrostatic energy and non-polar energy are contributed actively to the total interaction energy. In contrast, polar energy has a positive contribution to the whole interaction process. Based on the above

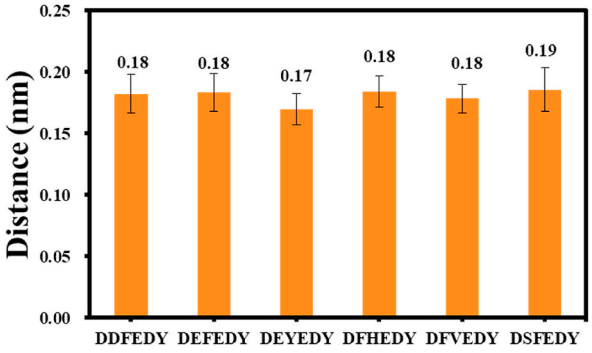

Fig. 6. The verification of the affinity. The average value of the minimum distance between short peptides and SARS-CoV-2 RBD during the whole simulation. The distance between the center of mass of the short peptide and the center of mass of SARS-CoV-2 RBD.

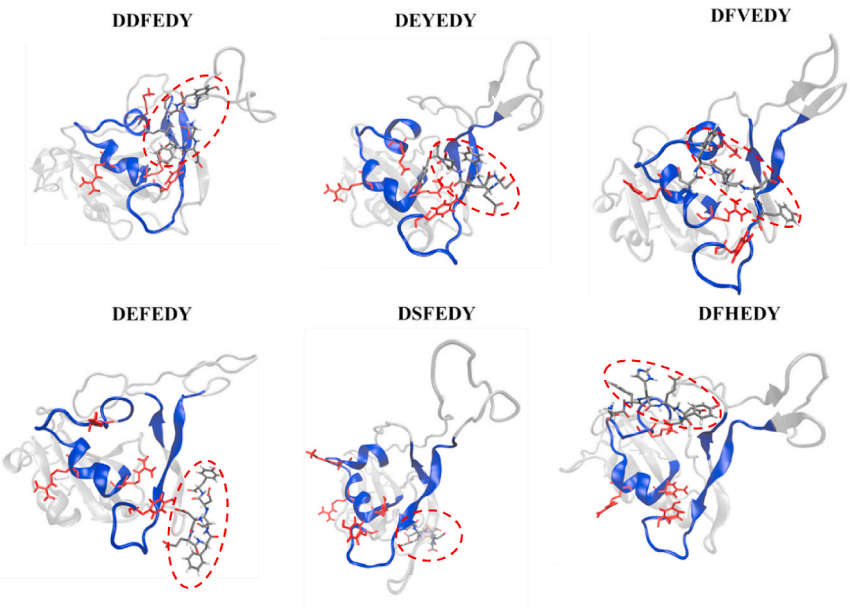

Fig. 7. The typical conformations of short peptides binding SARS-CoV-2 RBD at final 100 ns. The key residues of SARS-CoV-2 RBD were represented in red Licorice, the short peptides were represented in gray Licorice inside the red dashed line. SARS-CoV-2 RBD was displayed in blue and silver NewCartoon.

Table 2
The binding energies between the peptide inhibitors and ACE2 with SARS-CoV-2.

List of Systems under study	Van der Waal energy (kJ/mol)	Electrostatic energy (kJ/mol)	Polar solvation energy (kJ/mol)	SASA energy (kJ/mol)	Total binding energy (kJ/mol)
ACE2	−305.02 ± 19.75	−603.08 ± 72.94	583.51 ± 104.67	−40.10 ± 2.37	−364.70 ± 64.74
DEYEDY	−108.60 ± 21.60	−833.49 ± 104.80	502.67 ± 89.20	−17.24 ± 2.09	−456.66 ± 41.17
DDFEDY	−135.64 ± 19.07	−816.16 ± 81.22	583.66 ± 89.16	−20.78 ± 2.01	−388.92 ± 48.75
DFVEDY	−185.07 ± 20.33	−787.81 ± 73.18	680.23 ± 74.02	−23.24 ± 1.53	−315.87 ± 31.45

analysis, the *van der Waals*, electrostatic and non-polar interactions combinedly contribute to the stability of both the compounds. Thus, it was seen that the binding affinity of DEYEDY are the highest and DFVEDY the least among all the four systems under study.

3.6. Allergenicity, toxicity and solubility prediction

The allergenicity, toxicity, and solubility of above selected peptides were assessed via bioinformatics tools to endorse the validity and potency of the construct, some online networking tools were used. AllerTop V.2 and Toxinpred is widely used in antigenicity, sensitization, and toxicity analysis. It aims to predict allergens and non-allergens with high sensitivity and specificity [71]. Moreover, in addition to these parameters of peptides, the solubility of peptides is also important, good water solubility is also conducive to the role of peptides. Solubility is the measure of homogeneity of the system from the mixture of solute and solvent. It is considered as one of the vital parameters in drug concentration determination for a desired pharmacological response [56]. The studies [62,72] of Pei and Han designed new peptide inhibitors with seven residues based on the helical structure of ACE2. The allergenicity, toxicity, and solubility of these peptides were assessed (Table 3). However, QAKTFLD and GKGDFRI are predicted as possible allergens, and QAKTFLD peptide has been experimentally verified to have low cytotoxicity [62]. As for our peptides, they are non-immunogenic and non-toxic peptide. Due to AllerTOP V.2 was used to search for identical short (6–8) amino acid segments of the query protein and Toxinpred predicted a peptide sequence with length less than 50 residues, it is impossible to predict the allergenicity and toxicity of ΔABP-D25Y, LCB1, and LCB3. The results in Table 3 showed that DDFEDY, DEYEDY, and DFVEDY had no allergenicity, no toxicity and good water solubility, thus they would be excellent candidates to combat SARS-CoV-2.

The binding free energy calculations study have based MD simulation is the first step towards designing peptide inhibitors to block SARS-CoV-2 entry into the host cell. The use of peptides as therapeutics holds great promises for the treatment of continuously evolving viral infection of SARS-CoV-2 [73,74]. For example, Han et al. [75] designed peptide inhibitors extracted from the peptidase domain of ACE2 and simulated their interaction with the RBD of SARS-CoV-2 using molecular dynamics simulation. The results showed that $\alpha_{1,2}$-helixes peptides, which could provide a highly specific and stable binding to the RBD of SARS-CoV-2, suggesting that these peptides could be used as therapeutics against COVID-19. Maas et al. [76] designed and synthesized lactam-based, single stapled 35-mer

Table 3
The allergenicity, toxicity, and solubility profile of peptide inhibitors.

Peptides	Allergenicity	Toxicity	Solubility
DDFEDY	Non-Allergen	Non-Toxin	Good water solubility
DEYEDY	Non-Allergen	Non-Toxin	Good water solubility
DFVEDY	Non-Allergen	Non-Toxin	Good water solubility
QAKTFLD [62]	Defined as Allergen	Non-Toxin	Good water solubility
GKGDFRI [72]	Defined as Allergen	Non-Toxin	Good water solubility
ΔABP-D25Y [28]	No available	No available	Good water solubility
LCB1 [29]	No available	No available	Good water solubility
LCB3 [29]	No available	No available	Good water solubility

peptides based on the hACE2 N-terminal Helix 1 to interact directly with the SARS-CoV-2 RBD. It efficiently inhibits SARS-CoV-2 RBD-ACE2 binding and is resistant to degradation in the serum. However, in comparison with our structurally stable affinity peptide inhibitors (DX1X2EDY), they differ in structural stability, composition and molecular weight. The studies [75,76] conducted by Han and Maas show the design of new peptide inhibitors by mutations to the α-1 helix, with the presence of non-significant residues leading to deformity in its helical structure and longer peptide chain with larger molecular weight. Utilizing this fact in our study, each residue in the bind surface of the ACE2 was estimated for functional significance and structural stability based on their binding energy and conformational stability. We designed a molecular model for DX1X2EDY short peptide inhibitors where non-significant residues were truncated. Affinity peptide inhibitors have numerous major advantages over small size, small molecular weights, easy synthesis, with high specificity and affinity.

4. Conclusions

In this study, MD simulations and molecular docking were used to explore the interactions between SARS-CoV-2 RBD and ACE2 and design short peptide inhibitors with high affinity for SARS-CoV-2 RBD. The results of energy analysis between SARS-CoV-2 RBD and ACE2 report that both non-polar and polar energies are the main forces promoting their binding. Moreover, considering that there are many polar residues at their binding interface, and these polar residues contribute extremely high favorable energy, electrostatic energy also plays an important role. In addition, the key residues R403, R408, K417, and Y505 of SARS-CoV-2 RBD and the key residues D30, E37, D38, and Y41 of ACE2 were finally gained according to the results of energy analysis. And then, based on the distribution of key residues, short peptide inhibitors, including DDFEDY, DEFEDY, DEYEDY, DFVEDY, DFHEDY, and DSFEDY, with high affinity for SARS-CoV-2 RBD were constructed. Finally, MD simulation results of short peptides-SARS-CoV-2 RBD complex and the computer predictions suggest that DDFEDY, DEYEDY, and DFVEDY are expected to be effective inhibitors to prevent the protein-protein interactions between SARS-CoV-2 RBD and ACE2, thus preventing viral infection.

The sequence of SARS-CoV-2 has undergone frequent mutations, containing Alpha (B.1.1.7), Beta (B.1.351), Gamma (P.1), Delta (B.1.617.2), and Omicron (BA.1) variants [20]. These new variants may impair the efficacy of previously developed monoclonal antibody therapies [77]. Early data indicated that Omicron BA.2 sublineage had higher infectivity and more immune escape than the early wild-type (WT) strain, the previous variants of concern (VOCs), and BA.1 [78]. Cell culture infection assays [79,80] revealed that BA.2 variant was almost completely resistant to two therapeutic mAbs, casirivimab and idevimab, in contrast to their significant neutralizing activities against WT, Alpha, Gamma, and Delta. To test the efficacy of DDFEDY, DEYEDY, and DFVEDY, the large-scale analysis of variant protein structure docking has not been conducted yet. On the other hand, the methodological limitations stated above based on docking and simulation, the inhibitory potential of these short peptide in context to SARS-CoV-2 needs to be corroborated in further experimental attention. In addition, due to computational limitations, the prediction of allergenicity, toxicity and solubility of the affinity peptides also needs to be confirmed experimentally. It is recommended to compare our computational results with the designed peptides in vitro and in vivo, and eventually to clinical studies.

Author contribution statement

Xiaofeng Liu; Luying Jiang: Conceived and designed the experiments; Performed the experiments; Analyzed and interpreted the data; Wrote the paper.

Li Li; Fuping Lu; Fufeng Liu: Conceived and designed the experiments; Contributed reagents, materials, analysis tools or data.

Funding statement

Bionics design of affinity peptide inhibitors for Fufeng Liu was supported by the National Key R&D Program [No. 2018YFA0901700], the project of Novel Coronavirus Prevention and Treatment of Tianjin University of Science & Technology [No. 2020STCV0018].

Li Li was supported by the National Natural Science Foundation of China [No. 21908165].

Data availability statement

No data was used for the research described in the article.

Declaration of interest's statement

The authors declare no conflict of incomplex (kJ/mol)terest.

References

[1] A.E. Gorbalenya, S.C. Baker, R.S. Baric, et al., The species Severe acute respiratory syndrome-related coronavirus: classifying 2019-nCoV and naming it SARS-CoV-2, Nat Microbiol 5 (4) (2020) 536–544, https://doi.org/10.1038/s41564-020-0695-z.

[2] Coronaviridae Study Group of the International Committee on Taxonomy of, V, The species Severe acute respiratory syndrome-related coronavirus: classifying 2019-nCoV and naming it SARS-CoV-2, Nat Microbiol 5 (4) (2020) 536–544, https://doi.org/10.1038/s41564-020-0695-z.

[3] W. Cao, C. Dong, S. Kim, et al., Biomechanical characterization of SARS-CoV-2 spike RBD and human ACE2 protein-protein interaction, Biophys. J. 120 (6) (2021) 1011–1019, https://doi.org/10.1016/j.bpj.2021.02.007.

[4] S. Satarker, M. Nampoothiri, Structural proteins in severe acute respiratory syndrome coronavirus-2, Arch. Med. Res. 51 (6) (2020) 482–491, https://doi.org/10.1016/j.arcmed.2020.05.012.

[5] F. Li, Structure, function, and evolution of coronavirus spike proteins, Annu. Rev. Virol. 3 (1) (2016) 237–261, https://doi.org/10.1146/annurev-virology-110615-042301.

[6] F.F. Yan, F. Gao, Comparison of the binding characteristics of SARS-CoV and SARS-CoV-2 RBDs to ACE2 at different temperatures by MD simulations, Briefings Bioinf. 22 (2) (2021) 1122–1136, https://doi.org/10.1093/bib/bbab044.

[7] R. Yan, Y. Zhang, Y. Li, et al., Structural basis for the recognition of SARS-CoV-2 by full-length human ACE2, Science 367 (6485) (2020) 1444–1448, https://doi.org/10.1126/science.abb2762.

[8] Z.N. Zhao, J.Y. Zhou, M.X. Tian, et al., Omicron SARS-CoV-2 mutations stabilize spike up-RBD conformation and lead to a non-RBM-binding monoclonal antibody escape, Nat. Commun. 13 (1) (2022). ARTN 4958 10.1038/s41467-022-32665-7.

[9] W. Li, M.J. Moore, N. Vasilieva, et al., Angiotensin-converting enzyme 2 is a functional receptor for the SARS coronavirus, Nature 426 (6965) (2003) 450–454, https://doi.org/10.1038/nature02145.

[10] J. Lan, J. Ge, J. Yu, et al., Structure of the SARS-CoV-2 spike receptor-binding domain bound to the ACE2 receptor, Nature 581 (7807) (2020) 215–220, https://doi.org/10.1038/s41586-020-2180-5.

[11] F. Li, Receptor recognition mechanisms of coronaviruses: a decade of structural studies, J. Virol. 89 (4) (2015) 1954–1964, https://doi.org/10.1128/JVI.02615-14.

[12] M. Hoffmann, H. Kleine-Weber, S. Schroeder, et al., SARS-CoV-2 cell entry depends on ACE2 and TMPRSS2 and is blocked by a clinically proven protease inhibitor, Cell 181 (2) (2020) 271–280, https://doi.org/10.1016/j.cell.2020.02.052, e8.

[13] D. Wrapp, N. Wang, K.S. Corbett, et al., Cryo-EM structure of the 2019-nCoV spike in the prefusion conformation, Science 367 (6483) (2020) 1260–1263, https://doi.org/10.1126/science.abb2507.

[14] W. Li, C. Zhang, J. Sui, et al., Receptor and viral determinants of SARS-coronavirus adaptation to human ACE2, EMBO J. 24 (8) (2005) 1634–1643, https://doi.org/10.1038/sj.emboj.7600640.

[15] M. Ujike, C. Huang, K. Shirato, et al., Two palmitylated cysteine residues of the severe acute respiratory syndrome coronavirus spike (S) protein are critical for S incorporation into virus-like particles, but not for M-S co-localization, J. Gen. Virol. 93 (Pt 4) (2012) 823–828, https://doi.org/10.1099/vir.0.038091-0.

[16] X.X. Qu, P. Hao, X.J. Song, et al., Identification of two critical amino acid residues of the severe acute respiratory syndrome coronavirus spike protein for its variation in zoonotic tropism transition via a double substitution strategy, J. Biol. Chem. 280 (33) (2005) 29588–29595, https://doi.org/10.1074/jbc.M500662200.

[17] R.H. Hua, Y.F. Wang, Z.G. Bu, et al., Identification and antigenic epitope mapping of immunodominant region amino residues 510 to 672 on the spike protein of the severe acute respiratory syndrome coronavirus, DNA Cell Biol. 24 (8) (2005) 503–509, https://doi.org/10.1089/dna.2005.24.503.

[18] S.C. Lai, P.C. Chong, C.T. Yeh, et al., Characterization of neutralizing monoclonal antibodies recognizing a 15-residues epitope on the spike protein HR2 region of severe acute respiratory syndrome coronavirus (SARS-CoV), J. Biomed. Sci. 12 (5) (2005) 711–727, https://doi.org/10.1007/s11373-005-9004-3.

[19] Y. Cong, Y. Feng, H. Ni, et al., Anchor-locker binding mechanism of the coronavirus spike protein to human ACE2: insights from computational analysis, J. Chem. Inf. Model. 61 (7) (2021) 3529–3542, https://doi.org/10.1021/acs.jcim.1c00241.

[20] A.K. Padhi, S.L. Rath, T. Tripathi, Accelerating COVID-19 research using molecular dynamics simulation, J. Phys. Chem. B 125 (32) (2021) 9078–9091, https://doi.org/10.1021/acs.jpcb.1c04556.

[21] N. Mandal, A.K. Padhi, S.L. Rath, Molecular insights into the differential dynamics of SARS-CoV-2 variants of concern, J. Mol. Graph. Model. 114 (2022), 108194, https://doi.org/10.1016/j.jmgm.2022.108194.

[22] S.L. Rath, A.K. Padhi, N. Mandal, Scanning the RBD-ACE2 molecular interactions in Omicron variant, Biochem. Biophys. Res. Commun. 592 (2022) 18–23, https://doi.org/10.1016/j.bbrc.2022.01.006.

[23] V. Tragni, F. Preziusi, L. Laera, et al., Modeling SARS-CoV-2 spike/ACE2 protein-protein interactions for predicting the binding affinity of new spike variants for ACE2, and novel ACE2 structurally related human protein targets, for COVID-19 handling in the 3PM context, EPMA J. 13 (1) (2022) 149–175, https://doi.org/10.1007/s13167-021-00267-w.

[24] R. Kumar, N.A. Murugan, V. Srivastava, Improved binding affinity of omicron's spike protein for the human angiotensin-converting enzyme 2 receptor is the key behind its increased virulence, Int. J. Mol. Sci. 23 (6) (2022), https://doi.org/10.3390/ijms23063409.

[25] S. Ahmad, H.W. Abbasi, S. Shahid, et al., Molecular docking, simulation and MM-PBSA studies of nigella sativa compounds: a computational quest to identify potential natural antiviral for COVID-19 treatment, J. Biomol. Struct. Dyn. 39 (12) (2021) 4225–4233, https://doi.org/10.1080/07391102.2020.1775129.

[26] V. Kumar, H. Liu, C. Wu, Drug repurposing against SARS-CoV-2 receptor binding domain using ensemble-based virtual screening and molecular dynamics simulations, Comput. Biol. Med. 135 (2021), 104634, https://doi.org/10.1016/j.compbiomed.2021.104634.

[27] B. Leader, Q.J. Baca, D.E. Golan, Protein therapeutics: a summary and pharmacological classification, Nat. Rev. Drug Discov. 7 (1) (2008) 21–39, https://doi.org/10.1038/nrd2399.

[28] G. Jaiswal, V. Kumar, In-silico design of a potential inhibitor of SARS-CoV-2 S protein, PLoS One 15 (10) (2020), e0240004, https://doi.org/10.1371/journal.pone.0240004.

[29] L. Cao, I. Goreshnik, B. Coventry, et al., De novo design of picomolar SARS-CoV-2 miniprotein inhibitors, Science 370 (6515) (2020) 426–431, https://doi.org/10.1126/science.abd9909.

[30] D.M.O. Campos, M.K.D. Silva, E.D. Barbosa, et al., Exploiting reverse vaccinology approach for the design of a multiepitope subunit vaccine against the major SARS-CoV-2 variants, Comput. Biol. Chem. 101 (2022), 107754, https://doi.org/10.1016/j.compbiolchem.2022.107754.

[31] N.A. Mahmoud, A.M. Elshafei, Y.A. Almofti, A novel strategy for developing vaccine candidate against Jaagsiekte sheep retrovirus from the envelope and gag proteins: an in-silico approach, BMC Vet. Res. 18 (1) (2022) 343, https://doi.org/10.1186/s12917-022-03431-0.

[32] S. Gupta, P. Kapoor, K. Chaudhary, et al., In silico approach for predicting toxicity of peptides and proteins, PLoS One 8 (9) (2013), e73957, https://doi.org/10.1371/journal.pone.0073957.

[33] Q. Wang, Y. Zhang, L. Wu, et al., Structural and functional basis of SARS-CoV-2 entry by using human ACE2, Cell 181 (4) (2020) 894–904.e9, https://doi.org/10.1016/j.cell.2020.03.045.

[34] M. Stroet, B. Caron, K.M. Visscher, et al., Automated Topology builder version 3.0: prediction of solvation free enthalpies in water and hexane, J. Chem. Theor. Comput. 14 (11) (2018) 5834–5845, https://doi.org/10.1021/acs.jctc.8b00768.

[35] N. Schmid, A.P. Eichenberger, A. Choutko, et al., Definition and testing of the GROMOS force-field versions 54A7 and 54B7, Eur. Biophys. J. 40 (7) (2011) 843–856, https://doi.org/10.1007/s00249-011-0700-9.

[36] D. Van Der Spoel, E. Lindahl, B. Hess, et al., GROMACS: fast, flexible, and free, J. Comput. Chem. 26 (16) (2005) 1701–1718, https://doi.org/10.1002/jcc.20291.

[37] M.F. Harrach, B. Drossel, Structure and dynamics of TIP3P, TIP4P, and TIP5P water near smooth and atomistic walls of different hydroaffinity, J. Chem. Phys. 140 (17) (2014), 174501, https://doi.org/10.1063/1.4872239.

[38] A.D. MacKerell, D. Bashford, M. Bellott, et al., All-atom empirical potential for molecular modeling and dynamics studies of proteins, J. Phys. Chem. B 102 (18) (1998) 3586–3616, https://doi.org/10.1021/jp973084f.

[39] D. Barash, L. Yang, X. Qian, T. Schlick, Inherent speedup limitations in multiple time step/particle mesh Ewald algorithms, J. Comput. Chem. 24 (1) (2003) 77–88, https://doi.org/10.1002/jcc.10196.

[40] G.V. Dedkov, A.A. Kyasov, Dynamical van der Waals atom-surface interaction, Surf. Sci. 605 (11–12) (2011) 1077–1081, https://doi.org/10.1016/j.susc.2011.03.008.

[41] J.Y. Xie, G.H. Ding, M. Karttunen, Molecular dynamics simulations of lipid membranes with lateral force: rupture and dynamic properties, Biochim. Biophys. Acta 1838 (3) (2014) 994–1002, https://doi.org/10.1016/j.bbamem.2013.12.011.

[42] S. Genheden, U. Ryde, The MM/PBSA and MM/GBSA methods to estimate ligand-binding affinities, Expet Opin. Drug Discov. 10 (5) (2015) 449–461, https://doi.org/10.1517/17460441.2015.1032936.

[43] R. Kumari, R. Kumar, C. Open Source Drug Discovery, A. Lynn, g_mmpbsa–a GROMACS tool for high-throughput MM-PBSA calculations, J. Chem. Inf. Model. 54 (7) (2014) 1951–1962, https://doi.org/10.1021/ci500020m.

[44] W. Humphrey, A. Dalke, K. Schulten, VMD: visual molecular dynamics, J. Mol. Graph. 14 (1) (1996) 33–38, https://doi.org/10.1016/0263-7855(96)00018-5, 27-38.

[45] G.M. Morris, R. Huey, W. Lindstrom, et al., AutoDock4 and AutoDockTools4: automated docking with selective receptor flexibility, J. Comput. Chem. 30 (16) (2009) 2785–2791, https://doi.org/10.1002/jcc.21256.

[46] B. Huang, F.F. Liu, X.Y. Dong, Y. Sun, Molecular mechanism of the affinity interactions between protein A and human immunoglobulin G1 revealed by molecular simulations, J. Phys. Chem. B 115 (14) (2011) 4168–4176, https://doi.org/10.1021/jp111216g.

[47] T. Honma, Recent advances in de novo design strategy for practical lead identification, Med. Res. Rev. 23 (5) (2003) 606–632, https://doi.org/10.1002/med.10046.

[48] O. Trott, A.J. Olson, AutoDock Vina, Improving the speed and accuracy of docking with a new scoring function, efficient optimization, and multithreading, J. Comput. Chem. 31 (2) (2010) 455–461, https://doi.org/10.1002/jcc.21334.

[49] Y. Cao, Y. Chen, P. Wang, et al., Network pharmacology and experimental validation to explore the molecular mechanisms of Bushen Huoxue for the treatment of premature ovarian insufficiency, Bioengineered 12 (2) (2021) 10345–10362, https://doi.org/10.1080/21655979.2021.1996317.

[50] A.V. Sinitskiy, G.A. Voth, Quantum mechanics/coarse-grained molecular mechanics (QM/CG-MM), J. Chem. Phys. 148 (1) (2018), 014102, https://doi.org/10.1063/1.5006810.

[51] A. Sayyed-Ahmad, K. Tuncay, P.J. Ortoleva, Efficient solution technique for solving the Poisson-Boltzmann equation, J. Comput. Chem. 25 (8) (2004) 1068–1074, https://doi.org/10.1002/jcc.20039.

[52] O.V. Tsodikov, M.T. Record Jr., Y.V. Sergeev, Novel computer program for fast exact calculation of accessible and molecular surface areas and average surface curvature, J. Comput. Chem. 23 (6) (2002) 600–609, https://doi.org/10.1002/jcc.10061.

[53] D. Li, P. Chen, T. Shi, et al., HD5 and LL-37 inhibit SARS-CoV and SARS-CoV-2 binding to human ACE2 by molecular simulation, Interdiscip. Sci. 13 (4) (2021) 766–777, https://doi.org/10.1007/s12539-021-00462-3.

[54] I. Dimitrov, I. Bangov, D.R. Flower, I. Doytchinova, v AllerTOP, 2–a server for in silico prediction of allergens, J. Mol. Model. 20 (6) (2014) 2278, https://doi.org/10.1007/s00894-014-2278-5.

[55] S. Gupta, P. Kapoor, K. Chaudhary, et al., Peptide toxicity prediction, Methods Mol. Biol. 1268 (2015) 143–157, https://doi.org/10.1007/978-1-4939-2285-7_7.

[56] K.T. Savjani, A.K. Gajjar, J.K. Savjani, Drug solubility: importance and enhancement techniques, ISRN Pharm. 2012 (2012), 195727, https://doi.org/10.5402/2012/195727.

[57] C.A.S. Bergstrom, P. Larsson, Computational prediction of drug solubility in water-based systems: qualitative and quantitative approaches used in the current drug discovery and development setting, Int. J. Pharm. 540 (1–2) (2018) 185–193, https://doi.org/10.1016/j.ijpharm.2018.01.044.

[58] F.F. Liu, Z. Liu, S. Bai, et al., Exploring the inter-molecular interactions in amyloid-beta protofibril with molecular dynamics simulations and molecular mechanics Poisson-Boltzmann surface area free energy calculations, J. Chem. Phys. 136 (14) (2012), 145101, https://doi.org/10.1063/1.3702195.

[59] H. Zhang, J. Sang, L. Li, et al., Molecular basis for the inhibitory effects of 5-hydroxycyclopenicillone on the conformational transition of Abeta40 monomer, J. Biomol. Struct. Dyn. 39 (17) (2021) 6440–6451, https://doi.org/10.1080/07391102.2020.1799863.

[60] Y. Cao, J. Ge, Study of specific receptor binding mode suggests a possible enzymatic disinfectant for SARS-CoV-2, Langmuir 37 (5) (2021) 1707–1713, https://doi.org/10.1021/acs.langmuir.0c02911.

[61] F. Jafary, S. Jafari, M.R. Ganjalikhany, In silico investigation of critical binding pattern in SARS-CoV-2 spike protein with angiotensin-converting enzyme 2, Sci. Rep. 11 (1) (2021) 6927, https://doi.org/10.1038/s41598-021-86380-2.

[62] P. Pei, H. Qin, J. Chen, et al., Computational design of ultrashort peptide inhibitors of the receptor-binding domain of the SARS-CoV-2 S protein, Briefings Bioinf. 22 (6) (2021), https://doi.org/10.1093/bib/bbab243.

[63] Y. Wang, M. Liu, J. Gao, Enhanced receptor binding of SARS-CoV-2 through networks of hydrogen-bonding and hydrophobic interactions, Proc. Natl. Acad. Sci. U. S. A. 117 (25) (2020) 13967–13974, https://doi.org/10.1073/pnas.2008209117.

[64] F. Yan, F. Gao, RBD-ACE2 binding properties in five SARS-CoV-2 variants of concern with new perspectives in the design of pan-coronavirus peptide inhibitors, J. Infect. (2022), https://doi.org/10.1016/j.jinf.2022.09.011.

[65] Z. Wang, H. Sun, X. Yao, et al., Comprehensive evaluation of ten docking programs on a diverse set of protein-ligand complexes: the prediction accuracy of sampling power and scoring power, Phys. Chem. Chem. Phys. 18 (18) (2016) 12964–12975, https://doi.org/10.1039/c6cp01555g.

[66] E. Yuriev, J. Holien, P.A. Ramsland, Improvements, trends, and new ideas in molecular docking: 2012-2013 in review, J. Mol. Recogn. 28 (10) (2015) 581–604, https://doi.org/10.1002/jmr.2471.

[67] X. Hou, J. Du, J. Zhang, et al., How to improve docking accuracy of AutoDock4.2: a case study using different electrostatic potentials, J. Chem. Inf. Model. 53 (1) (2013) 188–200, https://doi.org/10.1021/ci300417y.

[68] F.F. Liu, X.Y. Dong, T. Wang, Y. Sun, Rational design of peptide ligand for affinity chromatography of tissue-type plasminogen activator by the combination of docking and molecular dynamics simulations, J. Chromatogr. A 1175 (2) (2007) 249–258, https://doi.org/10.1016/j.chroma.2007.10.074.

[69] H.R. Bairagya, B.P. Mukhopadhyay, S. Bhattacharya, Role of the conserved water molecules in the binding of inhibitor to IMPDH-II (human): a study on the water mimic inhibitor design, J. Mol. Struc. Theochem. 908 (1–3) (2009) 31–39, https://doi.org/10.1016/j.theochem.2009.04.037.

[70] P.J. Stansfeld, R. Hopkinson, F.M. Ashcroft, M.S. Sansom, PIP(2)-binding site in Kir channels: definition by multiscale biomolecular simulations, Biochemistry 48 (46) (2009) 10926–10933, https://doi.org/10.1021/bi9013193.

[71] I. Dimitrov, D.R. Flower, I. Doytchinova, AllerTOP–a server for in silico prediction of allergens, BMC Bioinf. 14 (Suppl 6) (2013) S4, https://doi.org/10.1186/1471-2105-14-S6-S4.

[72] S. Han, G. Zhao, Z. Wei, et al., An angiotensin-converting enzyme-2-derived heptapeptide GK-7 for SARS-CoV-2 spike blockade, Peptides 145 (2021), 170638, https://doi.org/10.1016/j.peptides.2021.170638.

[73] D. Schutz, Y.B. Ruiz-Blanco, J. Munch, et al., Peptide and peptide-based inhibitors of SARS-CoV-2 entry, Adv. Drug Deliv. Rev. 167 (2020) 47–65, https://doi.org/10.1016/j.addr.2020.11.007.
[74] C. Wang, S. Wang, D. Li, et al., Human intestinal defensin 5 inhibits SARS-CoV-2 invasion by cloaking ACE2, Gastroenterology 159 (3) (2020) 1145–1147, https://doi.org/10.1053/j.gastro.2020.05.015, e4.
[75] Y. Han, P. Kral, Computational design of ACE2-based peptide inhibitors of SARS-CoV-2, ACS Nano 14 (4) (2020) 5143–5147, https://doi.org/10.1021/acsnano.0c02857.
[76] M.N. Maas, J.C.J. Hintzen, P.M.G. Loffler, J. Mecinovic, Targeting SARS-CoV-2 spike protein by stapled hACE2 peptides, Chem. Commun. 57 (26) (2021) 3283–3286, https://doi.org/10.1039/d0cc08387a.
[77] D. Mannar, J.W. Saville, X. Zhu, et al., SARS-CoV-2 Omicron variant: antibody evasion and cryo-EM structure of spike protein-ACE2 complex, Science 375 (6582) (2022) 760–764, https://doi.org/10.1126/science.abn7760.
[78] Y. Zhou, H. Zhi, Y. Teng, The outbreak of SARS-CoV-2 Omicron lineages, immune escape, and vaccine effectivity, J. Med. Virol. (2022), https://doi.org/10.1002/jmv.28138.
[79] A. Chaqroun, C. Hartard, E. Schvoerer, Anti-SARS-CoV-2 vaccines and monoclonal antibodies facing viral variants, Viruses 13 (6) (2021), https://doi.org/10.3390/v13061171.
[80] A. Wilhelm, M. Widera, K. Grikscheit, et al., Limited neutralisation of the SARS-CoV-2 Omicron subvariants BA.1 and BA.2 by convalescent and vaccine serum and monoclonal antibodies, EBioMedicine 82 (2022), 104158, https://doi.org/10.1016/j.ebiom.2022.104158.